The Assembly of a Multisubunit Photosynthetic Membrane Protein Complex: A Site-Specific Spin Labeling EPR Spectroscopic Study of the PsaC Subunit in Photosystem I

4 AUTHORS, INCLUDING:

Bharat Jagannathan
University of California, Berkeley
12 PUBLICATIONS **97** CITATIONS

SEE PROFILE

K. V. Lakshmi
Rensselaer Polytechnic Institute
78 PUBLICATIONS **2,412** CITATIONS

SEE PROFILE

BIOCHEMISTRY
including biophysical chemistry & molecular biology

Article

The Assembly of a Multisubunit Photosynthetic Membrane Protein Complex: A Site-Specific Spin Labeling EPR Spectroscopic Study of the PsaC Subunit in Photosystem I[†]

Bharat Jagannathan,[‡] Sarah Dekat,[§] John H. Golbeck,[‡,||] and K. V. Lakshmi*,[§]

[‡]*Department of Biochemistry and Molecular Biology, and* [||]*Department of Chemistry, The Pennsylvania State University, University Park, Pennsylvania 16802, and* [§]*Department of Chemistry and Chemical Biology and The Baruch '60 Center for Biochemical Solar Energy Research, Rensselaer Polytechnic Institute, Troy, New York 12180*

ABSTRACT: The assembly of the PsaC subunit in the photosystem I (PS I) complex was studied using site-specific spin labeling electron paramagnetic resonance (EPR) spectroscopic techniques. The binding was monitored from the perspective of a reporter spin label attached to either the native $C34_C$ or the engineered $C75_C$ residue of wild-type PsaC ($PsaC_{WT}$). Three distinct stages of PsaC assembly were analyzed: unbound PsaC, the P_{700}-F_X/PsaC complex, and the P_{700}-F_X/PsaC/PsaD complex. The changes in the EPR spectral line shape and the rotational correlation time of the spin label when $PsaC_{WT}$ binds to the PS I core are consistent with the conformational changes that are expected to occur during the assembly process. The addition of the PsaD subunit to the P_{700}-F_X/$PsaC_{WT-C34}$ complex induces further EPR spectral changes, which indicate that the presence of PsaD affects the orientation of the PsaC subunit on the PS I core. The binding of several PsaC variants, each lacking one or more key binding contacts with the PsaA/PsaB heterodimer, was monitored using a reporter spin label at $C34_C$. Our results indicate that the absence of the PsaC-PsaA/PsaB binding contacts causes PsaC to bind in an altered configuration on the PS I core. In particular, the removal of the entire C-terminus ($PsaC_{C-term}$) causes PsaC to dock in a significantly different orientation when compared to the wild-type protein, as indicated by the EPR spectrum of the P_{700}-F_X/$PsaC_{C-term-C34}$ complex. Because the $PsaC_{C-term}$ variant retains only the symmetric network of PsaC-PsaA/PsaB ionic contacts, the altered EPR spectrum could, in principle, reflect a fraction of reaction centers that contain PsaC bound in the 180°-rotated, C_2-symmetry-related configuration. The results of this study are used to provide a comprehensive, stepwise mechanism for the binding of PsaC on the PS I core.

Photosystem I (PS I)[1] is a transmembrane protein−pigment complex that is vital for the process of oxygenic photosynthesis, the biochemical process by which solar energy is converted into chemical energy in cyanobacteria and higher plants. PS I catalyzes the light-induced electron transfer from the lumenal (inside the thylakoid membrane) donor, plastocyanin or cytochrome *c*, across the photosynthetic membrane to the stromal (outside the thylakoid membrane) acceptor, ferredoxin. Cyanobacterial PS I exists in a trimeric form, in which each monomer contains 12 protein subunits, 96 chlorophyll *a* molecules, 21 β-carotenes, 4 lipids, 2 phylloquinones, and 3 [4Fe-4S] clusters (*1*). Nine of the 12 subunits (PsaA, PsaB, PsaF, PsaI, PsaJ, PsaK, PsaL, PsaM, and PsaX) are primarily α-helical polypeptides that span the membrane. The PsaC, PsaD, and PsaE subunits do not contain transmembrane helices and are bound to the stromal surface of PS I, forming the "stromal hump" which provides the docking surface for soluble acceptors like ferredoxin and flavodoxin (*2, 3*).

The PsaA (83 kDa) and PsaB (83 kDa) subunits form the heterodimeric core of the PS I reaction center and contain most of the antenna pigments and electron transport cofactors. The electron transfer chain starts at a special pair of chlorophyll *a* (Chl *a*) molecules, P_{700}, named for its peak absorbance in the visible region. When P_{700} becomes photoexcited to the singlet state, its electron is transferred to the primary acceptor, A_0, a Chl *a* monomer (see ref *4* for an alternate hypothesis). The $P_{700}^+A_0^-$ charge-separated state is stabilized by rapid transfer of the electron to a bound phylloquinone (A_1) and then to a series of [4Fe-4S] clusters, F_X, F_A, and F_B, which function as an electron transfer wire (*5*). The terminal electron acceptors, F_A and F_B, are located in the PsaC subunit on the stromal side of the membrane. The organic cofactors of the electron transport chain in PS I are arranged in two symmetric branches along the PsaA and PsaB subunits. The two branches converge at F_X, and subsequent electron transfer to F_A and F_B is linear.

The two branches of electron transfer are in nearly perfect C_2 symmetry; the intercofactor distances are very nearly identical in both of the branches (*1*), and the cofactors in each of the branches are located at almost equal distances from the PsaA/PsaB interface. However, the PsaA and PsaB subunits are not precisely identical, and hence the system is best described as pseudo-C_2 symmetric. The axis of C_2 symmetry is positioned along the PsaA/PsaB interface and passes through the center of the F_X cluster and P_{700}. Although the C_2 symmetry weakens as

[1]Abbreviations: PS I, photosystem I; P_{700}, special pair of donor chlorophyll *a* molecules; Chl *a*, chlorophyll *a*; F_X, F_A, and F_B, [4Fe-4S] clusters X, A, and B, respectively; MTSL, (1-oxy-2,2,5,5-tetramethyl-3-pyrroline-3-methyl)methanethiosulfonate; EPR, electron paramagnetic resonance; τ_c, rotational correlation time.

the distance from the electron transport cofactors increases, the PsaA/PsaB heterodimer maintains a moderate degree of overall C_2 symmetry. The strong symmetry between the redox cofactors is broken by the PsaC subunit that contains the F_A and F_B iron−sulfur clusters; F_A and F_B are located at different distances from the F_X cluster and from the nearest symmetry-related phylloquinone in either the PsaA (A_{1A}) or PsaB (A_{1B}) subunit (1).

PsaC (9 kDa), PsaD (15 kDa), and PsaE (8 kDa) are soluble proteins that dock on the stromal surface of PS I. *In vitro* rebinding studies (6−8) and *in vivo* genetic deletion studies (9−11) suggest that the membrane-intrinsic portion of PS I (PS I core or the P_{700}-F_X complex) is assembled first and that the stromal subunits are subsequently assembled in a well-defined order: PsaC first, followed by PsaD and then PsaE. EPR spectroscopic evidence indicates that the F_A and F_B clusters in PsaC attain their final magnetic properties only after the binding of PsaD (6).

The PsaC subunit is bound to the PsaA/PsaB heterodimer primarily via an intricate network of ionic bonds between Arg/Lys residues on PsaC and Asp residues on PsaA/PsaB, the latter of which are part of the loop region that coordinates the F_X cluster (12, 13). The network of Arg/Lys-Asp ionic contacts is highly C_2 symmetric, i.e., the ionic PsaC-PsaA contacts appear very similar to the ionic PsaC-PsaB contacts. $R52_C$ on PsaC forms five ionic bonds with $D568_A/D579_A$ on PsaA, and $K51_C$/$R65_C$ on PsaC form five ionic bonds with $D555_B/D566_B$ on PsaB (12). Because the arrangement of the bonding Asp residues on PsaA/PsaB is so symmetric, the question arises as to how PsaC is able to distinguish between the Asp residues on PsaA and the Asp residues on PsaB during stromal assembly. If the network of ionic bonds were to be interchanged from the PsaA side to the PsaB side and vice versa, the resulting orientation of PsaC could be 180° rotated from its native orientation. The altered orientation of PsaC would likely preclude the binding of PsaD (12), which in turn would hinder the docking of soluble acceptors such as ferredoxin.

The only symmetry-breaking contacts between PsaC and the PsaA/PsaB heterodimer are the three H-bonds formed between $T73_C/Y80_C$ on the C-terminus of PsaC and $Q678_B/K702_B/P703_B$ on PsaB (12). Unlike the symmetric ionic contacts, a symmetry-related network of H-bonds does not exist on the PsaA subunit. Thus, the three H-bonds between the C-terminus of PsaC and PsaB are highly specific and are likely the key to the asymmetric binding of PsaC. It has thus been postulated that the binding of the C-terminus could be the determinant for the correct orientation of PsaC during the initial stages of the assembly process and that the symmetric ionic contacts are formed subsequently (12−14).

The role of the PsaD subunit in the stromal assembly process remains unclear. The C-terminus of PsaD wraps itself around PsaC and enhances the molecular interactions of the PsaC subunit with the PsaA/PsaB heteodimer (1). Analyses of the X-ray crystal structures of the PS I complex reveal that two-thirds of PsaD-PsaA/PsaB contacts would be disrupted if PsaD were to bind to a P_{700}-F_X/rotated PsaC complex (12). In principle, it is possible that the presence of PsaD could influence the correct assembly of the PsaC subunit. Furthermore, the binding of PsaD is functionally relevant; F_A and F_B attain their final magnetic properties only after PsaD binds (6), and only with PsaD bound are F_A and F_B able to reduce ferredoxin (2, 15).

The elucidation of the assembly pathways of multisubunit membrane proteins is of growing interest in structural biology. Very few attempts have been made to understand the dynamics of the PS I stromal assembly process, which is surprising given that high-resolution structures are available for the unbound and PS I-bound states of the PsaC subunit (1, 16). Site-specific spin labeling EPR spectroscopy is a powerful experimental tool for investigating protein structure and dynamics that uses either native or engineered cysteine residues (17, 18). The technique is particularly useful for studying the conformational dynamics of membrane-bound proteins (19, 20), which can be especially difficult to monitor using conventional techniques such as NMR spectroscopy. Based on the rigidity of the spin label, it is usually possible to detect the steric restrictions imposed by the environment of the label or the motion of a polypeptide backbone.

In this study, we observe the binding of PsaC to the PS I core (also referred to as P_{700}-F_X core) using spin labeling EPR spectroscopic techniques. The three stages of assembly (unbound PsaC, P_{700}-F_X/PsaC complexes, and P_{700}-F_X/PsaC/PsaD complexes) were monitored for wild-type PsaC ($PsaC_{WT}$) using a reporter spin label either at the native $C34_C$ or at the engineered $C75_C$ residue. The solution NMR structure of unbound PsaC and the X-ray crystal structure of the intact PS I-bound PsaC complex provide insight into the conformational changes that might occur during the assembly process (1, 12, 16). The iron−sulfur core of PsaC is rigid and remains relatively unchanged during the assembly process. However, the N- and the C-termini undergo significant conformational changes when PsaC binds to the PS I core (Figure 1). The placement of a reporter spin label at the native $C34_C$ residue on PsaC provides a probe for monitoring the dynamics of the loop region that connects the F_B and F_A binding site (16). The loop region is suggested to participate in the docking of flavodoxin/ferredoxin to PS I (3, 21). The attachment of a spin label at the engineered $C75_C$ position on PsaC provides an excellent probe on the role of the C-terminus of PsaC in locating the binding pocket on PsaB during the stromal assembly process (12−14).
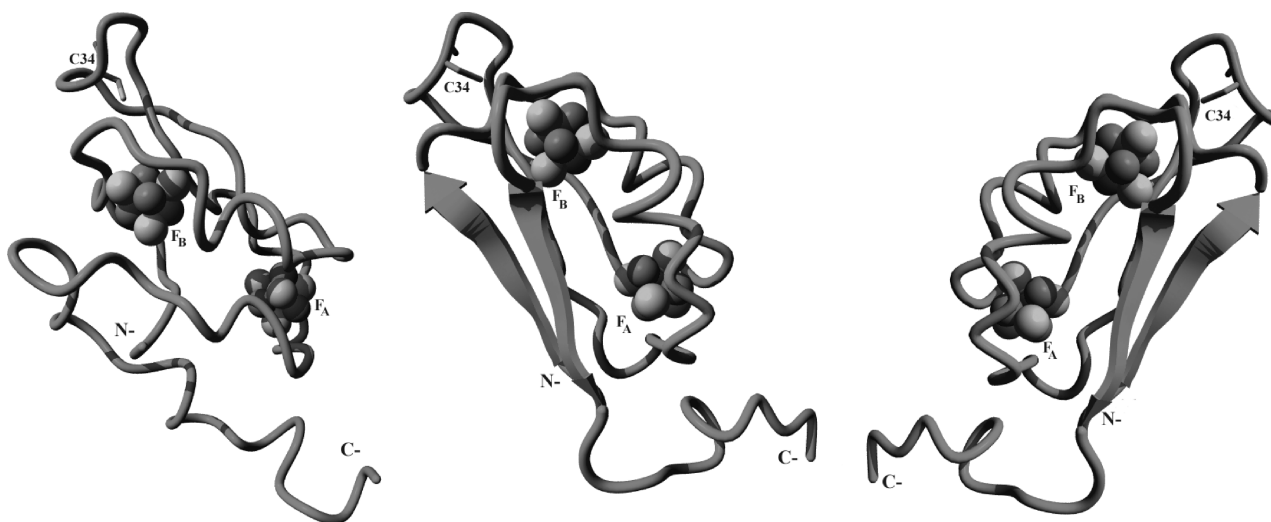
In addition to monitoring the conformational dynamics of $PsaC_{WT}$ assembly, the binding of several PsaC variants, each lacking one or more key binding contacts with the PsaA/PsaB heterodimer, was studied using a reporter spin label at the native $C34_C$ residue. The EPR spectra of spin-labeled variant PsaC during the different stages of assembly suggest an altered binding of these variant proteins to the PS I core. The results of this study are used to provide a comprehensive, stepwise mechanism for the binding of PsaC on the PS I core.

MATERIALS AND METHODS

Isolation of Intact PS I Complexes and Preparation of PS I Cores. PS I complexes were isolated from *Synechococcus* sp. PCC 7002 using Triton X-100 and purified by density gradient ultracentrifugation (6). The stromal subunits were removed by adding 6.8 M urea to intact PS I complexes, yielding P_{700}-F_X cores (7).

Site-Directed Mutagenesis of the psaC Gene. The site-directed *psaC* mutants were generated using the QuikChange site-directed mutagenesis kit (Stratagene, La Jolla, CA). PCR primers were designed on the basis of the sequence of the *psaC* gene from *Synechococcus* sp. PCC 7002. The mutant *psaC* constructs were verified by DNA sequencing. The plasmids were subsequently transformed into BL21-DE3 *Escherichia coli* competent cells for protein expression.

Recombinant Protein Purification and Reconstitution. Recombinant PsaC (wild-type and variant) and PsaD were

FIGURE 1: Structural differences between unbound PsaC (left, PDB ID: IK0T) and PS I-bound PsaC (middle, PDB ID: IJB0). The 180°-rotated orientation of PS I-bound PsaC is also shown (right). The native C34$_C$ residue is highlighted in the three structures and the iron−sulfur clusters, F$_A$ and F$_B$, are rendered as space-filling models. The N- and the C-termini are indicated in the three structures.

expressed in *E. coli* and purified as previously described (*8*). The iron−sulfur clusters were incorporated into the apo-PsaC protein by the addition of FeCl$_3$, Na$_2$S, and β-mercaptoethanol (*16*).

Preparation of Spin-Labeled PsaC Proteins. Since the [4Fe-4S] clusters in unbound PsaC are sensitive to oxidative degradation (*22*, *23*), all manipulations were performed in an anaerobic chamber with an atmosphere of 10% hydrogen and 90% nitrogen (Coy Laboratories, Grass Lake, MI). Prior to spin labeling, the holo-PsaC protein was incubated with 5 mM dithiothreitol for 1 h. The PsaC sample was then passed through three successive PD-10 desalting columns (GE Life Sciences, Piscataway, NJ) to remove excess dithiothreitol. The desalted protein was incubated at 4 °C with a 2-fold molar excess of (1-oxy-2,2,5,5-tetramethyl-3-pyrroline-3-methyl)methanethiosulfonate (MTSL) for 12 h. A second aliquot of MTSL, equivalent to the first, was subsequently added, and the reaction was allowed to continue for 4 h. Excess MTSL was removed from the protein sample by elution through three successive PD-10 desalting columns. The buffer used in all of the protein manipulations was 50 mM Tris-HCl at pH 8.2.

Reconstitution of P$_{700}$-F$_X$ Complexes with Spin-Labeled PsaC and PsaD. For the measurements on the P$_{700}$-F$_X$/spin-labeled PsaC complexes, a 3-fold molar excess of PsaC was added to P$_{700}$-F$_X$ complexes, and the excess PsaC was removed by repeated dilution and concentration over a Centricon filter device with a 100 kDa cutoff membrane. To study the P$_{700}$-F$_X$/spin-labeled PsaC/PsaD complexes, a 3-fold molar excess of PsaD was added to the washed P$_{700}$-F$_X$/spin-labeled PsaC complexes. The mixtures were incubated in the dark and transferred to 2 mm quartz tubes. All sample manipulations were performed under anaerobic conditions. The buffer contained 50 mM Tris-HCl, pH 8.2, 0.04% Triton X-100, and 20% glycerol.

X-Band Continuous-Wave EPR Spectroscopy. The EPR spectra were recorded on a custom-built cw/pulsed X-band Bruker Elexsys 580 spectrometer (Bruker BioSpin Corporation) with an ER4116DM dual-mode resonator equipped with a E-900 helium-flow cryostat (Oxford Instruments) and a quartz variable temperature dewar insert. For the room temperature (23 °C) measurements, the spin-labeled PsaC protein samples were loaded in 2 mm quartz capillaries under strictly anaerobic conditions using a LabConco protective glovebox. The total

sample volume was 20 μL. Typically 64 scans were averaged for each sample (scan width, 200 G) at a microwave power of 2 mW and 1 G modulation at 100 kHz modulation frequency.

EPR Spectral Simulations. The line shape simulations of the EPR spectra of the spin label in unbound PsaC, P$_{700}$-F$_X$/PsaC complexes, and P$_{700}$-F$_X$/PsaC/PsaD complexes were performed using a nonlinear least-squares (NLSL) fitting routine. The NLSL spectral fitting program, provided by Professor D. E. Budil (Northeastern University), uses a modified Levenberg−Marquardt algorithm (*24*). This program iterates the fitting procedure until a minimum in the least-squares fit is achieved. The values for the *g*-tensor (g_{xx}, g_{yy}, and g_{zz}) and the hyperfine coupling constants in the *A*-tensor (A_{xx}, A_{yy}, and A_{zz} for nitrogen-14) were optimized manually. The geometric average rotational rates (rbar(1) and rbar(2)) and the Gaussian inhomogeneous line broadening (gib0) were treated as variables in the fitting routine. The values of rbar(1), rbar(2), and gib0 were varied to find the least-squares best fit given the fixed *g*-tensor and *A*-tensor values. The *g*-tensor and *A*-tensor values were varied reiteratively, and the spectral simulations were reevaluated to best fit the experimental data. The residual index, reduced χ^2 value, and a qualitative comparison of the simulated spectrum with the experimental spectrum were used to determine the best fit. The output of the spectral fitting program provided the rotational correlation times and the relative populations of the two components used to fit the experimental data.

Typically, each spectrum was fit with two independent sites having different isotropic mobilities and variable populations. Each spectral fit yielded a fast component with rotational correlation times of ∼2.5 ns, which represents the free or nonspecifically bound spin label that is present in solution (see Results). Although it is desirable to further desalt and/or dialyze the sample to remove the residual free spin label in solution, these manipulations are tedious under anaerobic conditions, and there is a risk of denaturing the iron−sulfur clusters in PsaC upon exposure to molecular oxygen. The slow component with longer rotational correlation times arises from the MTSL spin label that is bound to specific cysteine sites on the PsaC protein. In each case, the two-component fit adequately accounts for the narrow (free spin label) and broad (PsaC-bound spin label) resonances observed in the experimental EPR spectra. For the sake of clarity,
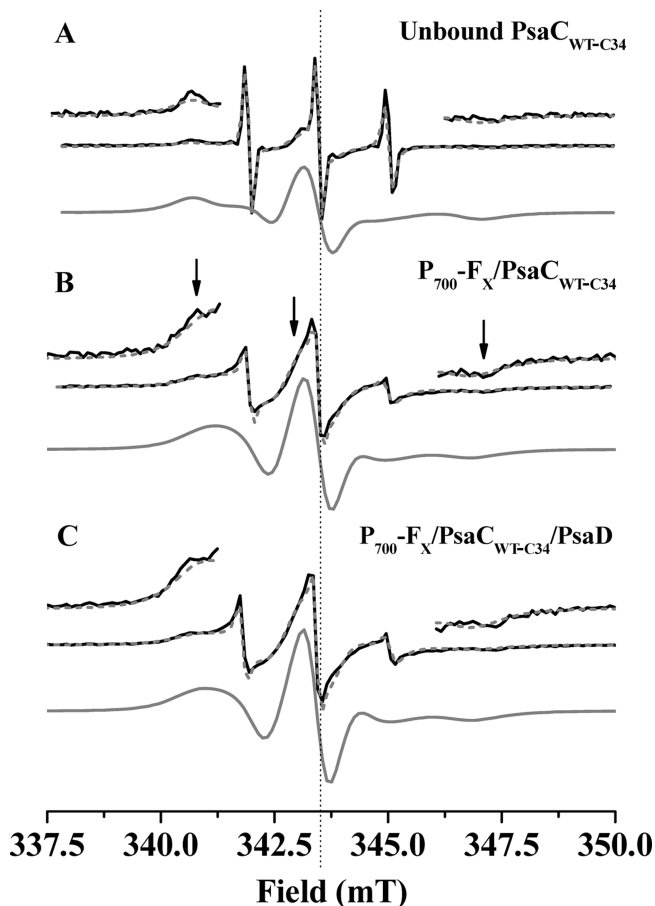
FIGURE 2: Experimental (solid black line) and simulated (dashed gray line) EPR spectra of the spin label in (A) unbound $PsaC_{WT-C34}$, (B) P_{700}-F_X/$PsaC_{WT-C34}$ complexes, and (C) P_{700}-F_X/$PsaC_{WT-C34}$/PsaD complexes. Also shown are spectral simulations of the broad component (solid gray line) arising from the PsaC-bound spin label in spectra A−C.

Table 1: Rotational Correlation Times (τ_c, in ns) of the PsaC-Bound Spin Label Obtained by Spectral Simulation of the EPR Spectra for Unbound $PsaC_{WT}$, P_{700}-F_X/$PsaC_{WT}$ Complexes, and P_{700}-F_X/$PsaC_{WT}$/PsaD Complexes[a]

complex	$PsaC_{WT-C34}$		$PsaC_{WT-C75}$	
	τ_c (ns)	ΔH_0, H^2	τ_c (ns)	ΔH_0, H^2
unbound PsaC	6.5 (80%)	8.48, 330	4.9 (80%)	6.85, 312
P_{700}-F_X/PsaC	3.7 (90%)	6.21, 294	4.5 (85%)	6.60, 309
P_{700}-F_X/PsaC/PsaD	4.0 (90%)	6.50, 309	4.1 (90%)	6.45, 286

[a]$PsaC_{WT}$ was spin-labeled at two separate sites, C34$_C$ and C75$_C$. The values indicated in parentheses represent the fraction of the total EPR signal that can be attributed to the PsaC-bound spin label. The remainder of the signal is accounted for by free spin label in solution with a significantly faster τ_c and is not shown for the sake of clarity. Also presented are the central line widths (ΔH_0 (G)) and the spectral second moments (H^2 (G^2)) obtained from the experimental EPR spectra of the PsaC-bound spin label.

the experimental and simulated composite EPR spectra as well as the simulated broad component due to the protein-bound spin label are shown for each sample.

RESULTS

Assembly of Wild-Type PsaC on the P_{700}-F_X Core. Figure 2A shows the EPR spectrum of the MTSL reporter spin label that is covalently bound to the native C34$_C$ residue of unbound $PsaC_{WT}$ ($PsaC_{WT-C34}$). The experimental and simulated EPR spectra display overlapping broad and narrow components arising from the spin label. Each spectrum was fit with two independent sites with different isotropic rotational mobilities and variable populations. Also shown is the simulated EPR spectral line shape of the broad component of the spin label. The broad component represents the fraction of the spin label that is covalently bound to PsaC and accounts for nearly 80% of the EPR signal with a rotational correlation time (τ_c) of 6.5 ns (Table 1). The observed τ_c is consistent with an EPR spectral line shape arising from a moderately immobilized nitroxide spin label as reported by Jordan and co-workers (*25*). Thus, it appears that the labeling procedure causes a predominant fraction of the spin label to be covalently linked to PsaC. The narrow component of the spectrum relaxes considerably faster (τ_c = 2.5 ns) and accounts for the remaining 20% of the EPR signal. The narrow component can arise due to three populations of the label: (i) free,

residual spin label in solution; (ii) spin label that is nonspecifically bound to PsaC; (iii) spin label that is covalently bound to apo-PsaC, which has lost its iron−sulfur clusters due to oxidative degradation. Although the labeling procedure was performed under strictly anaerobic conditions (<5 ppm oxygen), it is possible that a small fraction of clusters got degraded during the handling of the sample. Because PsaC loses its native protein fold in the absence of the clusters, a spin label covalently bound to apo-PsaC would have a higher rotational mobility when compared to holo-PsaC.

As shown in Figure 2B, the addition of $PsaC_{WT-C34}$ to P_{700}-F_X cores causes a dramatic change in the line shape of the EPR spectrum of the spin label. The line width of the PsaC-bound spin label component (highlighted by arrows) is substantially different in P_{700}-F_X/$PsaC_{WT-C34}$ complexes when compared to unbound $PsaC_{WT-C34}$. This change is further highlighted in the simulated EPR spectral line shape of the PsaC-bound spin label component that is also shown in Figure 2B. The spectral changes are indicative of a significant difference in the environment of the reporter spin label at C34$_C$ between the unbound and PS I core-bound states. The τ_c obtained from spectral line shape simulations of P_{700}-F_X/$PsaC_{WT-C34}$ complexes is 3.7 ns, which is a 45% decrease when compared to unbound $PsaC_{WT-C34}$ (Table 1). The decrease in the τ_c value is likely caused due to an increased mobility of the MTSL nitroxide side chain at C34$_C$ when PsaC binds to the PS I core. A small fraction of the label (∼10%) exhibits a faster τ_c of 2.5 ns, which could represent free MTSL, nonspecifically bound MTSL, or MTSL covalently linked to apo-$PsaC_{WT-C34}$. The decrease in the amount of free label when compared to $PsaC_{WT-C34}$ is likely due to the repeated dilution and concentration of the P_{700}-F_X/$PsaC_{WT-C34}$ complexes that was performed to eliminate unbound $PsaC_{WT-C34}$.

The addition of PsaD to P_{700}-F_X/$PsaC_{WT-C34}$ complexes results in subtle changes in the EPR spectral line shape of the spin label (Figure 2C). The spectral simulations indicate that the τ_c increases from 3.7 ns for P_{700}-F_X/$PsaC_{WT-C34}$ complexes to 4.0 ns for P_{700}-F_X/$PsaC_{WT-C34}$/PsaD complexes, indicating a slight decrease in the mobility of the nitroxide spin label due to the binding of the PsaD subunit. The changes in spectral line shape observed for P_{700}-F_X/$PsaC_{WT-C34}$/PsaD complexes are consistent with previous low-temperature EPR studies that suggest a slight change in the configuration of PsaC on the PS I core upon the binding of PsaD (*6*).

Also shown in Figure 2 are the vertically expanded outer spectral regions of both the experimental and simulated EPR

spectra of the reporter spin label that is covalently bound to the native $C34_C$ residue of unbound $PsaC_{WT}$. A careful comparison of the outer edges of the expanded experimental and simulated spectra reveals a slight mismatch of the spectral features. The overall motion of the reporter spin label that is covalently attached to the protein is characterized by the frequency, amplitude, and anisotropy of the rotational motion of the spin label. The frequency and amplitude of the rotational reorientation of the reporter spin label are adequately accounted for in the spectral simulations using "isotropic" mobilities. However, the effect of local ordering of the reporter spin label in the protein environment leads to rotational anisotropy that is not accounted for in the spectral simulations. It has been previously reported by Hubbell, Mchaourab, Perozo, and co-workers that the local microscopic ordering of the reporter spin label leads to restrictions in the conformational space due to interactions with neighboring side chains or backbone atoms. This is evidenced by averaging of the *g*- and hyperfine (*A*-) tensors (26−28). A semiempirical measure of spin label dynamics with local microscopic ordering can be obtained through the line shape parameter (ΔH_0) and the spectral second moment (H^2). The parameters, ΔH_0 and H^2, have been found to correlate with the binding site and environment of the reporter spin label where the magnitude of these parameters depends on the degree of averaging of the *g*- and *A*-tensors, respectively (26−28). The values of ΔH_0 and H^2 increase as the frequency of motion of the reporter spin label decreases, and the same is true for the increase in molecular ordering. Thus, ΔH_0 and H^2 can be used to probe the rate and anisotropy of rotational mobility. Shown in Table 1 are the values of the line shape parameter (ΔH_0) and the spectral second moment (H^2) of the MTSL reporter spin label that is covalently bound to the native $C34_C$ residue of unbound $PsaC_{WT}$, P_{700}-F_X/$PsaC_{WT}$ complexes, and P_{700}-F_X/$PsaC_{WT}$/PsaD complexes. The ΔH_0 and H^2 values of the native $C34_C$ residue in the unbound $PsaC_{WT}$ protein (ΔH_0 = 8.48 G and H^2 = 330 G^2) decrease when the $PsaC_{WT}$ binds to the P_{700}-F_X complex (ΔH_0 = 6.21 G and H^2 = 294 G^2). Furthermore, there is a slight increase of ΔH_0 and H^2 in the presence of the PsaD subunit (ΔH_0 = 6.50 G and H^2 = 309 G^2). This serves as independent confirmation of the dynamics of the reporter spin label at the native $C34_C$ residue of $PsaC_{WT}$ and provides a qualitative measure of the effects of molecular ordering on the reporter spin label. The mobility parameters obtained from the semiempirical analysis are in agreement with the trend of τ_c values that are obtained by the spectral fitting program fit using two independent sites with different isotropic rotational mobilities and variable populations (Table 1).

To observe the binding of PsaC from the perspective of its C-terminus, $S75_C$ was replaced with a Cys residue by site-directed mutagenesis. The native $C34_C$ was converted into a Ser residue, thus eliminating the possibility of the formation of doubly spin-labeled PsaC during the labeling procedure.

Figure 3A shows the experimental and simulated EPR spectra of the reporter spin label attached to $C75_C$ in unbound $PsaC_{WT}$ ($PsaC_{WT-C75}$). The composite spectra display both the narrow spectral component due to the free or nonspecifically bound spin label and the broad component (shown separately in Figure 3A) from the spin label bound to PsaC at $C75_C$. The EPR spectrum of unbound $PsaC_{WT-C75}$, in particular the low-field component, is distinct when compared to that of unbound $PsaC_{WT-C34}$ (Figures 3A and 2A). A τ_c of 4.9 ns is obtained for the EPR line shape arising from the spin label in $PsaC_{WT-C75}$, which is
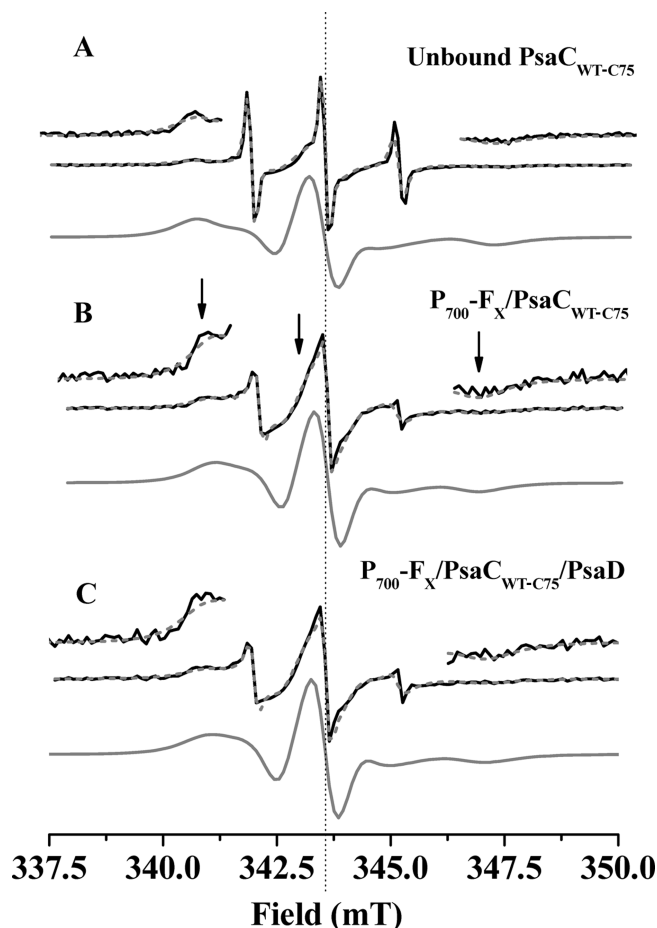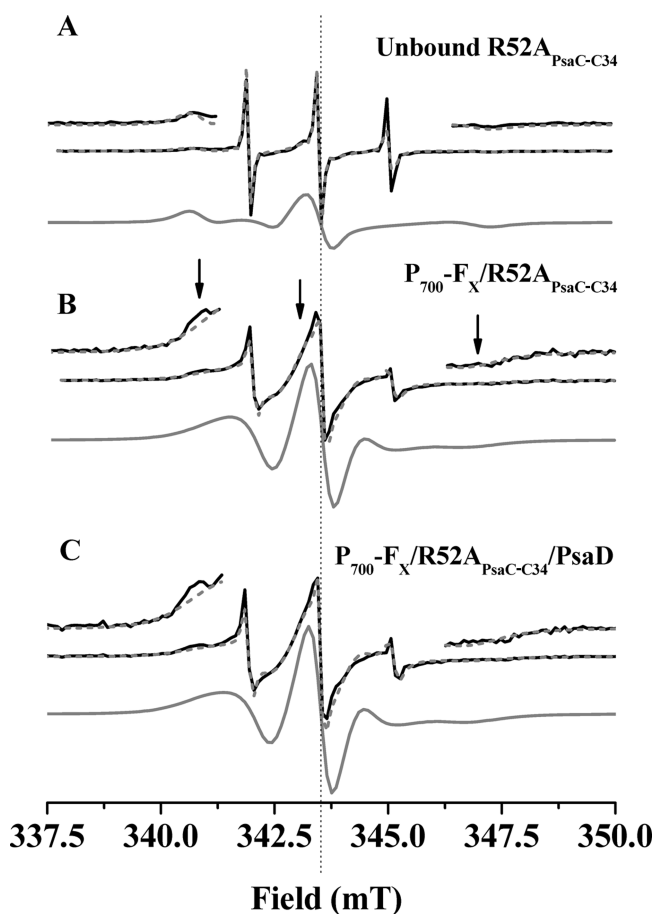

FIGURE 3: Experimental (solid black line) and simulated (dashed gray line) EPR spectra of the spin label in (A) unbound $PsaC_{WT-C75}$, (B) P_{700}-F_X/$PsaC_{WT-C75}$ complexes, and (C) P_{700}-F_X/$PsaC_{WT-C75}$/PsaD complexes. Also shown are spectral simulations of the broad component (solid gray line) arising from the PsaC-bound spin label in spectra A−C.

~25% lower when compared to the τ_c of the spin label in $PsaC_{WT-C34}$ (Table 1). The lower τ_c is indicative of an increased mobility of the spin label at $C75_C$ on the C-terminus of PsaC relative to $C34_C$, which is consistent with the flexibility of the C-terminus as observed in the solution NMR structure of unbound PsaC (16). However, the τ_c of the spin label in $PsaC_{WT-C75}$ is much slower than that of free or nonspecifically bound spin label (~2.5 ns), suggesting that the C-terminus of PsaC is not as highly disordered as implied by the solution NMR structures (16).

The addition of $PsaC_{WT-C75}$ to P_{700}-F_X cores causes significant changes in the spectral line width of the spin label (highlighted by arrows) (Figure 3B), indicative of alterations in the environment of the label upon the binding of PsaC. Quantitative spectral simulations show that the τ_c for the spin label in P_{700}-F_X/$PsaC_{WT-C75}$ complexes is 4.5 ns, which is ~10% lower than the observed τ_c in unbound $PsaC_{WT-C75}$ (Table 1). Although an increase in mobility appears to be a common feature for the spin label at $C34_C$ and $C75_C$ during the binding of PsaC to the PS I core, the magnitude of the increase is less profound at the latter position.

The addition of PsaD to P_{700}-F_X/$PsaC_{WT-C75}$ complexes resulted in very subtle changes in the EPR spectra of the spin label (Figure 3C). The τ_c of the spin label at $C75_C$ decreases from 4.5 ns in P_{700}-F_X/$PsaC_{WT-C75}$ complexes to 4.1 ns in P_{700}-F_X/$PsaC_{WT-C75}$/PsaD complexes, suggesting an increased mobility of the nitroxide spin label upon the binding of PsaD.

Shown in Figure 3 are the vertically expanded outer spectral regions of both the experimental and simulated spectra of the reporter spin label attached in PsaC$_{WT-C75}$. A comparison of the outer edges of the expanded experimental and simulated spectra reveals a slight mismatch of the spectral features. Shown in Table 1 are the values of the line shape parameter (ΔH_0) and the spectral second moment (H^2) of the spin label in unbound PsaC$_{WT-C75}$, the P$_{700}$-F$_X$/PsaC$_{WT-C75}$ complexes, and the P$_{700}$-F$_X$/PsaC$_{WT-C75}$/PsaD complexes. The ΔH_0 and H^2 values of the spin label in unbound PsaC$_{WT-C75}$ decrease when it binds to the P$_{700}$-F$_X$ complex and when PsaD is added to P$_{700}$-F$_X$/PsaC$_{WT-C75}$ complexes. The mobility parameters of the semiempirical

FIGURE 4: Experimental (solid black line) and simulated (dashed gray line) EPR spectra of the spin label in (A) unbound R52A$_{PsaC-C34}$, (B) P$_{700}$-F$_X$/R52A$_{PsaC-C34}$ complexes, and (C) P$_{700}$-F$_X$/R52A$_{PsaC-C34}$/PsaD complexes. Also shown are spectral simulations of the broad component (solid gray line) arising from the PsaC-bound spin label in spectra A−C.

analysis are consistent with the trend of τ_c values that are obtained by the spectral fitting program fit using two independent sites with different isotropic rotational mobilities and variable populations (Table 1).

Binding of Variant PsaC Proteins Lacking Symmetric Ionic Bond Forming Contacts with the PsaA/PsaB Heterodimer. The symmetric ionic contacts between PsaC and the PsaA/PsaB heterodimer have been proposed to play a critical role in the oxygen stability of PS I-bound PsaC (*29*). To better understand the role of the ionic contacts in the assembly process, we analyzed the binding of two PsaC variants, R52A$_{PsaC}$ and R65A$_{PsaC}$. The former variant lacks all five ionic bonds between PsaC and PsaA, and the latter lacks four of the five ionic bonds between PsaC and PsaB (*12, 13*). In both instances, the reporter spin label was covalently linked to the native C34$_C$ residue (R52A$_{PsaC-C34}$ and R65A$_{PsaC-C34}$).

The EPR spectrum of unbound R52A$_{PsaC-C34}$ (Figure 4A) is qualitatively similar to that of unbound PsaC$_{WT-C34}$, which is consistent with the orientation of C34$_C$ remaining unaffected by a point mutation in the binding region. The experimental and simulated EPR spectra display overlapping narrow and broad components, similar to the features observed in PsaC$_{WT-C34}$. The broad component due to the PsaC-bound spin label (Figure 4A, solid gray line) accounts for nearly 85% of the total EPR signal with a rotational correlation time, τ_c, of 8.5 ns (Table 2), which is consistent with an EPR spectral line shape of a moderately immobilized nitroxide spin label. However, it is interesting that the τ_c of the spin label in R52A$_{PsaC-C34}$ is significantly slower than the τ_c in PsaC$_{WT-C34}$ (6.5 ns).

As shown in Figure 4B, there is a profound change in the line width of the spin label in R52A$_{PsaC-C34}$ (highlighted by arrows) upon association with the P$_{700}$-F$_X$ complex. The spectral alteration is better observed in the simulated line shape of the broad component shown in Figure 4B (solid gray line). A quantitative analysis from EPR spectral simulations indicates that the binding of the R52A$_{PsaC-C34}$ is accompanied by an ~60% decrease in τ_c for the label (8.5 ns in unbound R52A$_{PsaC-C34}$ compared to 3.3 ns in P$_{700}$-F$_X$/R52A$_{PsaC-C34}$ complexes). Qualitatively, the EPR spectrum of P$_{700}$-F$_X$/R52A$_{PsaC-C34}$ complexes is only slightly different than that of P$_{700}$-F$_X$/PsaC$_{WT-C34}$ complexes, suggesting that the absence of PsaC-PsaA contacts does not significantly affect the orientation of PsaC on the stromal surface.

The addition of PsaD to P$_{700}$-F$_X$/R52A$_{PsaC-C34}$ complexes causes subtle spectral changes (Figure 4C) to the line shape of the spin label, indicating that the absence of PsaC-PsaA contacts likely does not preclude the assembly of PsaD. EPR spectral simulations indicate that the τ_c of the spin label in P$_{700}$-F$_X$/R52A$_{PsaC-C34}$/PsaD complexes is 3.5 ns, which is an ~5%

Table 2: Rotational Correlation Times (τ_c, in ns) of the PsaC-Bound Spin Label Obtained by Spectral Simulation of the EPR Spectra for the Different Stages of Assembly in the R52A$_{PsaC}$, R65A$_{PsaC}$, and PsaC$_{C-term}$ Variants of PsaC[a]

complex	R52A$_{PsaC-C34}$		R65A$_{PsaC-C34}$		PsaC$_{C-term-C34}$	
	τ_c (ns)	$\Delta H_0, H^2$	τ_c (ns)	$\Delta H_0, H^2$	τ_c (ns)	$\Delta H_0, H^2$
unbound PsaC	8.5 (85%)	9.40, 350	9.8 (75%)	9.76, 354	5.7 (85%)	7.70, 340
P$_{700}$-F$_X$/PsaC	3.3 (90%)	5.80, 270	5.4 (85%)	7.40, 319	4.3 (90%)	6.50, 293
P$_{700}$-F$_X$/PsaC/PsaD	3.5 (90%)	5.96, 280	4.9 (90%)	7.10, 302	4.4 (95%)	6.60, 303

[a]The variant proteins were spin-labeled at the native C34$_C$ residue. The values indicated in parentheses represent the fraction of the total EPR signal that can be attributed to the PsaC-bound spin label. The remainder of the signal is accounted for by free spin label in solution with a significantly faster τ_c and is not shown for the sake of clarity. Also presented are the central line widths (ΔH_0 (G)) and the spectral second moments (H^2 (G^2)) obtained from the experimental EPR spectra of the PsaC-bound spin label.
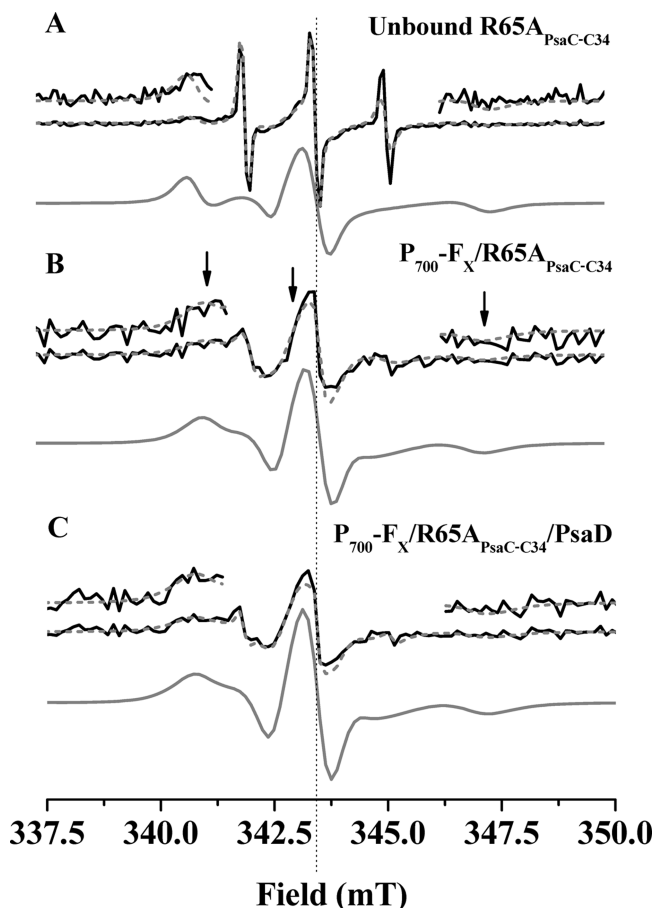
FIGURE 5: Experimental (solid black line) and simulated (dashed gray line) EPR spectra of the spin label in (A) unbound $R65A_{PsaC-C34}$, (B) P_{700}-F_X/$R65A_{PsaC-C34}$ complexes, and (C) P_{700}-F_X/$R65A_{PsaC-C34}$/PsaD complexes. Also shown are spectral simulations of the broad component (solid gray line) arising from the PsaC-bound spin label in spectra A−C.

increase when compared to P_{700}-F_X/$R52A_{PsaC-C34}$ complexes (Table 2). It should be noted that the trend of changes in the τ_c values during the three stages of $R52A_{PsaC-C34}$ assembly is comparable to $PsaC_{WT-C34}$.

A comparison of the vertically expanded outer edges of the expanded experimental and simulated spectra reveals a slight mismatch of the spectral features (Figure 4). Table 2 shows the values of the line shape parameter (ΔH_0) and the spectral second moment (H^2) of the MTSL reporter spin label in unbound $R52A_{PsaC-C34}$, the P_{700}-F_X/$R52A_{PsaC-C34}$ complexes, and the P_{700}-F_X/$R52A_{PsaC-C34}$/PsaD complexes. The ΔH_0 and H^2 values of the $C34_C$ residue in unbound $R52A_{PsaC-C34}$ decrease upon binding to the P_{700}-F_X core, and there is a slight increase in these values when PsaD is added to P_{700}-F_X/$R52A_{PsaC-C34}$ complexes. The mobility parameters of the semiempirical analysis are consistent with the trend of τ_c values that are obtained by the spectral fitting program fit using two independent sites with different isotropic rotational mobilities and variable populations (Table 2).

As shown in Figure 5A, the EPR spectrum of unbound $R65A_{PsaC-C34}$ is very similar to that of $PsaC_{WT-C34}$. The broad component of the PsaC-bound spin label (Figure 5A, solid gray line) accounts for nearly 75% of the EPR signal with a rotational correlation time of 9.8 ns (Table 2).

The addition of $R65A_{PsaC-C34}$ to P_{700}-F_X core complexes causes significant spectral changes (Figure 5B) and is accompa-

nied by a decrease in the correlation time to 5.4 ns. The EPR spectrum of P_{700}-F_X/$R65A_{PsaC-C34}$ complexes is significantly different than P_{700}-F_X/$PsaC_{WT-C34}$ complexes (Figure 2B), indicating that the absence of four PsaC-PsaB ionic contacts causes PsaC to bind in a markedly altered configuration on the PS I core.

The addition of PsaD to P_{700}-F_X/$R65A_{PsaC-C34}$ complexes causes subtle EPR spectral changes (Figure 5C), which suggests that PsaD influences the orientation of this PsaC variant on the PS I core. Quantitative spectral simulations of P_{700}-F_X/$R65A_{PsaC-C34}$/PsaD complexes provide a τ_c of 4.9 ns for the spin label, which is lower than the observed τ_c of 5.4 ns in P_{700}-F_X/$R65A_{PsaC-C34}$ complexes. This is contrary to the trend in PS I core complexes that were reconstituted with $PsaC_{WT-C34}$ and $R52A_{PsaC-C34}$, wherein the addition of PsaD is accompanied by a decrease in the mobility of the spin label nitroxide side chain.

A comparison of the vertically expanded outer edges of the expanded experimental and simulated spectra reveals a slight mismatch of the spectral features (Figure 5). Shown in Table 2 are the values of the line shape parameter (ΔH_0) and the spectral second moment (H^2) of the spin label that is covalently bound to $C34_C$ in unbound $R65A_{PsaC-C34}$, P_{700}-F_X/$R65A_{PsaC-C34}$ complexes, and P_{700}-F_X/$R65A_{PsaC-C34}$/PsaD complexes. The ΔH_0 and H^2 values of the $C34_C$ residue in the unbound $R65A_{PsaC-C34}$ protein decrease when the $R65A_{PsaC-C34}$ binds to the P_{700}-F_X and P_{700}-F_X/PsaD complexes. The mobility parameters of the semiempirical analysis mirror the trend of τ_c values that are obtained by the spectral fitting program fit using two independent sites with different isotropic rotational mobilities and variable populations (Table 2).

Binding of a PsaC Variant Lacking the Symmetry-Breaking Contacts with the PsaA/PsaB Heterodimer. It has previously been proposed that the formation of three symmetry-breaking hydrogen bonds between $T73_C$/$Y80_C$ on PsaC and $Q678_B$/$K702_B$/$P703_B$ on PsaB and hydrophobic interactions between a Gly-Leu-Ala-Tyr sequence on the C-terminus of PsaC and the Pro-Val-Ala-Leu hydrophobic pocket on PsaB could drive the binding of the two proteins (*12, 13*). To test this prediction, the C-terminus deletion variant of PsaC ($PsaC_{C-term}$) was constructed that was devoid of residues 71−80 and thus lacks all of the symmetry-breaking interactions with PsaB. This PsaC variant ($PsaC_{C-term}$) contains only the C_2-symmetric network of ionic contacts and was spin-labeled at the native $C34_C$ position ($PsaC_{C-term-C34}$) like the other site-directed variants.

As shown in Figure 6A, the EPR spectrum of unbound $PsaC_{C-term-C34}$ has spectral features that are very similar to those of unbound $PsaC_{WT-C34}$, which indicates that the removal of the C-terminus does not affect the immediate environment of the spin label. The correlation time of the spin label in unbound $PsaC_{C-term-C34}$ is 5.7 ns (Table 2), which is slightly lower than the value observed for unbound $PsaC_{WT-C34}$.

Interestingly, this variant is capable of binding to PS I cores, albeit in a significantly different configuration, as indicated by the altered EPR spectrum for P_{700}-F_X/$PsaC_{C-term-C34}$ complexes (Figure 6B) when compared to P_{700}-F_X/$PsaC_{WT-C34}$ complexes (Figure 2B). The τ_c values of the label in $PsaC_{C-term-C34}$ follow a similar trend as $PsaC_{WT-C34}$; there is a decrease from 5.7 to 4.3 ns during the binding of the protein to the PS I core (Table 2).

The addition of PsaD to P_{700}-F_X/$PsaC_{C-term-C34}$ complexes results in negligible changes to the spectral features (Figure 6C) and the correlation times (Table 2). This observation suggests that PsaD does not play a role in stabilizing the $PsaC_{C-term}$ variant on the PS I core and that it is possibly not involved in
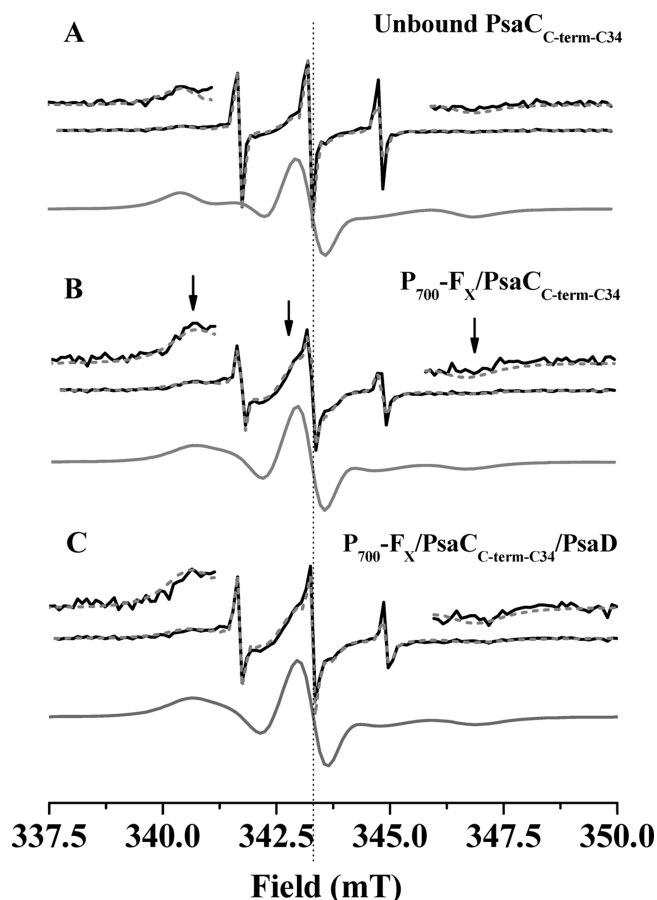
FIGURE 6: Experimental (solid black line) and simulated (dashed gray line) EPR spectra of the spin label in (A) unbound PsaC$_{C-term-C34}$, (B) P$_{700}$-F$_X$/PsaC$_{C-term-C34}$ complexes, and (C) P$_{700}$-F$_X$/PsaC$_{C-term-C34}$/PsaD complexes. Also shown are spectral simulations of the broad component (solid gray line) arising from the PsaC-bound spin label in spectra A−C.

positioning PsaC to attain the correct orientation in the absence of the symmetry-breaking contacts (see Discussion).

Shown in Figure 6 are the vertically expanded outer spectral regions of both the experimental and simulated spectra. A comparison of the outer edges of the expanded experimental and simulated spectra reveals a slight mismatch of the spectral features. Shown in Table 2 are the values of the line shape parameter (ΔH_0) and the spectral second moment (H^2) of the reporter spin label in unbound PsaC$_{C-term}$, the P$_{700}$-F$_X$/PsaC$_{C-term}$ complexes, and the P$_{700}$-F$_X$/PsaC$_{C-term}$/PsaD complexes. The ΔH_0 and H^2 values of the C34$_C$ residue in the unbound PsaC$_{C-term}$ protein decrease when it binds to the P$_{700}$-F$_X$ complex. However, there is a slight increase in ΔH_0 and H^2 values of the C34$_C$ residue in the P$_{700}$-F$_X$/PsaC$_{C-term}$ complex in the presence of PsaD. The mobility parameters of the semiempirical analysis are in excellent agreement with the trend of τ_c values that are obtained by the spectral fitting program fit using two independent sites with different isotropic rotational mobilities and variable populations (Table 2).

Based on the results of the present study, it appears that the removal of R65$_C$ or the C-terminus leads to the most profound change in the orientation of PS I-bound PsaC when compared to the other site-directed mutations.

DISCUSSION

Assembly of Wild-Type PsaC on the PS I Core. A comparison of the solution NMR structure of unbound PsaC and the X-ray crystal structure of the intact PS I-bound PsaC complex provides insight into the conformational changes that might occur during the assembly process (*1, 12, 16*). The iron−sulfur core of PsaC is rigid and remains relatively unchanged during the assembly process. However, the N- and the C-termini undergo significant conformational changes when PsaC binds to the PS I core. The C-terminus of PsaC, which exists in a coiled conformation in the unbound form, assumes an extended conformation in the PS I-bound state (Figure 1). In unbound PsaC, the N-terminus is positioned perpendicular to the pre-C-terminus (residues 65−70) and away from the F$_A$ cluster (*12, 16*). Upon binding to PS I, the N-terminus moves closer to the F$_A$ cluster and positions itself parallel to the pre-C-terminus, forming an antiparallel β-sheet (*1, 12*). The EPR spectra of spin-labeled PsaC during different stages of assembly correlate well with the predicted structural changes during the binding process.

In the first set of experiments, a spin label covalently attached to the native C34$_C$ residue on PsaC$_{WT}$ was used as a probe for monitoring the dynamics of the binding process. C34$_C$ is part of a loop region which follows the α-helical turn that connects the F$_B$ and F$_A$ binding sites (*16*). The loop region is reported to be involved in the docking of flavodoxin/ferredoxin to PS I (*3, 21*). There are several changes in the EPR spectrum of the spin label when PsaC$_{WT-C34}$ binds to the PS I core. Surprisingly, the rotational correlation time, τ_c, is lower for PS I-bound PsaC when compared to unbound PsaC. This is contrary to the expected increase in τ_c when a relatively small protein (PsaC, 10 kDa) associates with a large membrane protein complex (PS I core, ~330 kDa). Although the secondary structure and the position of the loop region are very similar in unbound and PS I-bound PsaC, there appears to be a subtle difference in the orientation of the C34$_C$ side chain between the two states of the protein (Figure 1). It should be noted that the dynamic fluctuations of the amino acid side chains are not usually evident in an X-ray crystal structure, which provides a rigid snapshot of the protein in its energy minimum state. However, based on the difference in rotational correlation times and semiempirical line shape parameters, it is reasonable to assume that the C34$_C$ side chain is relatively more solvent exposed in the PS I-bound state when compared to the unbound state, thus providing the spin label with more rotational mobility. The amount of conformational space explored by the label is relatively small when compared to the size of the protein, and a slight change in the local environment of the label is enough to induce significant changes in the rotational correlation times and line shape parameters.

The second set of experiments was performed with a PsaC variant that had a reporter label on a cysteine residue that was engineered into position 75 on the C-terminus of the protein. The native C34$_C$ was converted to a Ser residue by site-directed mutagenesis. The C-terminus of PsaC, which is helically disordered in the unbound form, assumes an extended conformation in the PS I-bound PsaC complex (*12*). The extension of the C-terminus is thought to assist PsaC in locating the binding pocket on PsaB during the stromal assembly (*12−14*). The lower τ_c, ΔH_0, and H^2 values for the spin label at C75$_C$ when compared to C34$_C$ correlate well with the increased flexibility of the C-terminus of unbound PsaC when compared to the more rigid secondary structure associated with the C34$_C$ position. Upon binding to the PS I core, there are spectral changes in the EPR line shape obtained from the spin label at C75$_C$, which likely arise due to alterations in the environment of the label when the C-terminus of PsaC uncoils during the assembly.

Role of PsaD in Stromal Assembly. The addition of PsaD to P_{700}-F_X/PsaC$_{WT-C34}$ complexes led to very subtle changes in the EPR spectra and τ_c values. The presence of PsaD restricts the mobility of the spin label at the C34$_C$ position, as indicated by an increase in τ_c, ΔH_0, and H^2 values observed for P_{700}-F_X/PsaC$_{WT-C34}$/PsaD complexes. The binding of PsaD is critical to the proper functioning of a photosynthetic cell as it, along with PsaC and PsaE, provides the binding surface for acceptor proteins such as ferredoxin and flavodoxin (*3, 30*). C34$_C$ is part of the solvent-exposed loop region in PsaC that is believed to be involved in interactions with ferredoxin (*16, 21*). It is reasonable to imagine that the binding of PsaD imparts rigidity to the loop region in PsaC, thus defining the docking site for ferredoxin.

The very minor changes in the spectral features of the PsaC-bound spin label, at both the C34$_C$ and C75$_C$ positions, upon the addition of PsaD are consistent with the proposal that PsaD acts to stabilize the PsaC subunit on the stromal surface of PS I (*12*). The results from the present study are in agreement with previous low-temperature EPR spectroscopy experiments, which indicate a slight alteration in the environment around the F_A and F_B iron−sulfur clusters in PsaC upon the addition of PsaD to P_{700}-F_X/PsaC complexes (*6*). There also have been suggestions that PsaD might be involved in determining the correct C_2-symmetric orientation of PsaC on PS I (*12*). However, *in vitro* resolution/reconstitution and *in vivo* genetic deletion studies clearly show that the presence of bound PsaC on the PS I core is a prerequisite for the binding of PsaD (*6, 9, 10*). As a result, PsaC must attain its orientation without any assistance from PsaD. The subtle changes in the EPR spectrum of the spin label and the previously observed minor alterations in the magnetic environment around the F_A and F_B clusters when PsaD binds to P_{700}-F_X/PsaC complexes suggest that it is more likely that PsaD is involved in "fine-tuning" the position of PsaC on PS I rather than determining its orientation.

Binding of Variant PsaC Proteins Lacking Symmetric Ionic Bond Forming Contacts with the PsaA/PsaB Heterodimer. In addition to analyzing the assembly of PsaC$_{WT}$ on the PS I core, we studied the binding of PsaC variants that lacked key ionic bond forming contacts with the PsaA/PsaB heterodimer. The significant spectral differences observed for the line shape of the spin label at C34$_C$ when PsaC binds to the PS I core made this residue a suitable reporter for the binding of the PsaC variants. It is difficult to introduce a spin label very close to the binding site, since two of the three positively charged amino acids on PsaC that form ionic bonds with PsaA/PsaB are part of the CxxCxxCxxxCP iron−sulfur cluster binding motif that coordinates the F_A cluster (*29*). The introduction of an extra Cys residue in a well-conserved cluster-ligating motif could disrupt the incorporation of the iron−sulfur clusters in PsaC and thus render the protein incapable of binding to the PS I core.

R52$_C$ forms five ionic bonds with D568$_A$/D579$_A$, and K51$_C$/R65$_C$ establish five ionic contacts with D555$_B$/D566$_B$ (*12*). The R52A$_{PsaC}$ variant was generated to eliminate all ionic contacts between PsaC and PsaA. Unexpectedly, this variant binds to PS I, albeit in a slightly different orientation when compared to PsaC$_{WT}$. It is very surprising that R52A$_{PsaC}$ is capable of assembling onto the PS I core, given that it cannot form one-half of the symmetric network of ionic contacts. The addition of PsaD seems to have a similar effect as was observed with PsaC$_{WT}$, suggesting that PsaD is capable of binding to the P_{700}-F_X/R52A$_{PsaC}$ complex. In the 2.5 Å X-ray crystal structure of PS I (PDB ID: 1JB0), the C-terminus of PsaD has extensive interactions with the N-terminal region of PsaC, which is positioned very close to the F_A cluster (*1, 12*). Because R52$_C$ is part of the F_A-coordinating CxxCxxCxxxCP motif, it seems possible that the extensive PsaC-PsaD contacts can stabilize PsaC in the absence of the PsaC-PsaA contacts.

The addition of R65A$_{PsaC-C34}$, which lacks four of the five ionic bonds with PsaB, to the PS I core resulted in very weak EPR resonances that were significantly different than those observed for P_{700}-F_X/PsaC$_{WT-C34}$ complexes. It appears that the absence of the four ionic contacts between PsaC and PsaB causes PsaC to bind in a significantly altered configuration on the PS I core when compared to the native protein.

It is interesting that the signal-to-noise (S/N) ratio of the EPR spectrum of P_{700}-F_X/R65A$_{PsaC-C34}$ complexes is lower than P_{700}-F_X/PsaC$_{WT-C34}$ and P_{700}-F_X/R52A$_{PsaC-C34}$ complexes. We suspect that the association of R65A$_{PsaC}$ with the PS I core is not as tight as the native protein and that the repeated dilution and concentration of P_{700}-F_X/R65A$_{PsaC-C34}$ complexes, meant to remove unbound R65A$_{PsaC-C34}$ from the sample mixture, also removed a significant proportion of loosely bound R65A$_{PsaC-C34}$. Since the major fraction of P_{700}-F_X cores likely does not contain bound R65A$_{PsaC}$, the EPR spectrum of P_{700}-F_X/R65A$_{PsaC-C34}$ complexes has a low S/N ratio when compared to reconstituted PS I complexes with PsaC$_{WT}$ and R52A$_{PsaC}$.

Based on these results, it appears that the removal of the PsaC-PsaB ionic contacts has a more deleterious effect on the binding of PsaC when compared to the PsaC-PsaA ionic contacts.

Existence of a P_{700}-F_X/Rotated PsaC Complex. In the absence of the C-terminus, the network of contacts between PsaC and the PsaA/PsaB heterodimer is perfectly C_2 symmetric. Thus, in theory, there exists the possibility of an 180°-rotated, symmetry-related orientation of the PsaC$_{C-term}$ variant when it binds to the PS I core (*12*). However, it has been proposed that the positioning of the N-terminus of PsaC, perpendicular to the pre-C-terminus (residues 65−70), ensures that K51$_C$, R52$_C$, and R65$_C$ are distant from the equilibrium positions that they attain in bound PsaC, thus precluding PsaC binding in the symmetric region (*13*). The repositioning of the N-terminus during the assembly process will allow the strands containing the bonding residues to relax and thus orient the positively charged residues correctly. However, 1 of the 30 solution NMR structures determined for unbound PsaC has the N-terminus positioned parallel to the pre-C-terminus (*16*), which would allow for PsaC binding in the symmetric region. Thus, it is possible that the N-terminus exists in a dynamic equilibrium with the pre-C-terminus and that, in theory, there may be a small probability of PsaC binding in the 180°-rotated orientation if the N-terminus is not positioned perpendicular to the pre-C-terminus.

The EPR spectrum of P_{700}-F_X/PsaC$_{C-term-C34}$ suggests that PsaC is able to bind to PS I cores in the absence of the C-terminus, albeit in a significantly different orientation than the native protein. Previous low-temperature EPR and time-resolved optical spectroscopic experiments have shown that PsaC forms a functional complex with the PS I membrane core even in the absence of the symmetry-breaking C-terminal tail (*29*). It is reasonable to assume that PsaC$_{C-term}$ is bound to the PS I core solely via the symmetric network of ionic bonds. Because the network of Arg/Lys-Asp contacts between PsaC and the PsaA/PsaB heterodimer is almost perfectly C_2 symmetric, PsaC$_{C-term}$ can bind in either of the two C_2-symmetry-related orientations shown in Figure 1. Thus, in principle, it is possible that a fraction of the *in vitro* reconstituted PS I complexes contain PsaC$_{C-term}$ in

the rotated orientation. However, in the absence of an X-ray crystal structure or additional studies of the P_{700}-F_X/rotated PsaC complex, it is difficult to unambiguously determine whether the altered EPR spectrum of the spin label reflects the rotated orientation of PsaC.

Insights into the Mechanism of PsaC Binding. The availability of high-resolution structures for unbound and PS I-bound PsaC has led to the development of several models for the binding of PsaC, with the focus primarily on whether the symmetric ionic bonds or the symmetry-breaking H-bonds are established first between PsaC and the PsaA/PsaB hetero-dimer (*12, 14*). Here, we use the results of the spin labeling EPR studies to propose a comprehensive, stepwise mechanism for the assembly of PsaC on the PS I core, starting with the assumption that the symmetric ionic bonds are not formed during the initial stages of binding. If the symmetric contacts were established first, there would be a possibility of PsaC binding in the 180°-rotated, C_2-symmetry-related configuration (Figure 1). Indeed, as indicated by the EPR spectrum of P_{700}-F_X/PsaC$_{C\text{-term-C34}}$ complexes, PsaC can bind in the absence of the symmetry-breaking C-terminal contacts, albeit in a non-native orientation. Because the C_2-symmetric network of PsaC-PsaA/PsaB ionic contacts can be formed equally well with PsaC bound in either orientation, the dissociation of the incorrectly bound PsaC will involve the breaking of several strong ionic bonds, which is likely a thermodynamically unfavorable process.

Thus, the first committed binding step would be the anchoring of the C-terminus of PsaC with the specific binding pocket on PsaB, thereby locking the "correct" orientation of PsaC at the onset of binding. The high degree of flexibility of the PsaC C-terminus, as indicated by the τ_c, ΔH_0, and H^2 values of the spin label in PsaC$_{WT\text{-C75}}$, would allow it to explore a relatively large amount of conformational space to locate its specific binding pocket on PsaB. The entropic driving force provided by the fusion of the hydrophobic surfaces on PsaB as well as the C-terminal region of PsaC is likely to be sufficiently strong to drive the binding process (*13*).

Once the C-terminal region of PsaC is bound to PsaB, the remaining contacts will be formed as the iron−sulfur core of the protein docks on the membrane surface. It is tempting to speculate that the ionic bonds are formed sequentially, with the first contact being established between the residue closest to the PsaC C-terminus, R65$_C$, and D555$_B$/D566$_B$ on PsaB. R65$_C$ is part of the pre-C-terminal region (residues 64−68) that forms an antiparallel β-sheet with the N-terminus in PS I-bound PsaC. The immobilization of the pre-C-terminal backbone via the forma-tion of strong ionic bonds between R65$_C$ and D555$_B$/D566$_B$ would position it to form multiple H-bonds with the N-terminal backbone, thereby providing an enthalpic driving force for the binding process. In this context, it is interesting that R65A$_{PsaC}$ appears to bind relatively loosely to the PS I core when compared to the other PsaC variants. According to this mechanism, R65A$_{PsaC}$ would be tethered solely via the symmetry-breaking contacts with PsaB, which might be responsible for the facile dissociation of the variant from the membrane core.

The final docking of PsaC might occur through ionic bond formation between R52$_C$ and D568$_A$/D579$_A$ PsaA and between K51$_C$ and D566$_B$. The free energy of docking would be driven by the enthalpic contribution of ionic bond formation and by the entropic contribution due to the displacement of water molecules that are structured near the hydrophobic regions of all three proteins. The relatively minor changes in the EPR spectrum of

P_{700}-F_X/R52A$_{PsaC\text{-C34}}$ complexes when compared to P_{700}-F_X/PsaC$_{WT\text{-C34}}$ complexes suggests that the orientation of PsaC is mostly determined prior to the formation of ionic bonds between PsaC and PsaA.

The minor spectral changes when PsaD is added to P_{700}-F_X/PsaC complexes indicate that PsaD influences the configuration of PsaC on the PS I core, although it is difficult to predict if the presence of PsaD is needed for the formation of final contacts between PsaC and the PsaA/PsaB heterodimer. Nevertheless, given the negligible changes in the spectral features and rotational correlation times of P_{700}-F_X/PsaC$_{C\text{-term-C34}}$ complexes upon the addition of PsaD, it appears that PsaD does not play a significant role in preventing the incorrect binding of PsaC. Instead, the presence of PsaD is likely more necessary to provide a docking surface for soluble acceptor proteins like ferredoxin.

To our knowledge, this is the first time that the assembly of a multisubunit membrane protein complex has been studied by spin labeling EPR techniques. Future studies will involve the attachment of double spin labels on PsaC to better comprehend the conformational changes that occur during the binding process. The alterations in the dipolar coupling between the two spins can provide a wealth of information on the conforma-tional changes that occur during the assembly process (*31*). For instance, the uncoiling of the PsaC C-terminus during binding can be monitored by doubly spin labeling the C-terminus (amino acids 71−80). In the unbound state, the distance between the spin labels will likely be shorter since the C-terminus exists in a helically coiled conformation. The extension of the C-terminus during the binding of PsaC will increase the distance between the two labels. The alterations in the dipolar coupling (and hence the distance) can be used to directly probe the conformational dynamics of the stepwise assembly process.

The methodology described in this study can be adopted to elucidate the assembly pathways of a variety of multisubunit protein complexes. The presence of a genetic transformation system is critical, given that several site-directed mutants might be required to comprehensively understand an assembly mecha-nism. Because many protein complexes do not have redox cofactors, spin labeling presents the best opportunity to compre-hend the sophisticated assembly pathways using biophysical techniques.

REFERENCES

1. Jordan, P., Fromme, P., Witt, H. T., Klukas, O., Saenger, W., and Krauss, N. (2001) Three dimensional structure of photosystem I at 2.5 Å resolution. *Nature 411*, 909–917.
2. Setif, P. (2001) Ferredoxin and flavodoxin reduction by photosystem I. *Biochim. Biophys. Acta 1507*, 161–179.
3. Setif, P., Fischer, N., Lagoutte, B., Bottin, H., and Rochaix, J. D. (2002) The ferredoxin docking site of photosystem I. *Biochim. Bio-phys. Acta 1555*, 204–209.
4. Holzwarth, A. R., Muller, M. G., Niklas, J., and Lubitz, W. (2006) Ultrafast transient absorption studies on photosystem I reaction centers from *Chlamydomonas reinhardtii*. 2: mutations near the P_{700} reaction center chlorophylls provide new insight into the nature of the primary electron donor. *Biophys. J. 90*, 552–565.

5. Brettel, K. (1997) Electron transfer and arrangement of the redox cofactors in photosystem I. *Biochim. Biophys. Acta 1318*, 322–373.

6. Li, N., Zhao, J. D., Warren, P. V., Warden, J. T., Bryant, D. A., and Golbeck, J. H. (1991) PsaD is required for the stable binding of PsaC to the photosystem I core protein of *Synechococcus* sp. PCC 6301. *Biochemistry 30*, 7863–7872.

7. Parrett, K. G., Mehari, T., Warren, P. G., and Golbeck, J. H. (1989) Purification and properties of the intact P_{700} and F_X-containing photosystem I core protein. *Biochim. Biophys. Acta 973*, 324–332.

8. Zhao, J., Warren, P. V., Li, N., Bryant, D. A., and Golbeck, J. H. (1990) Reconstitution of electron transport in photosystem I with PsaC and PsaD proteins expressed in *Escherichia coli. FEBS Lett. 276*, 175–180.

9. Yu, J., Smart, L. B., Jung, Y. S., Golbeck, J., and McIntosh, L. (1995) Absence of PsaC subunit allows assembly of photosystem I core but prevents the binding of PsaD and PsaE in *Synechocystis* sp. PCC 6803. *Plant Mol. Biol. 29*, 331–342.

10. Chitnis, V. P., Jung, Y. S., Albee, L., Golbeck, J. H., and Chitnis, P. R. (1996) Mutational analysis of photosystem I polypeptides—role of PsaD and the lysyl 106 residue in the reductase activity of photosystem I. *J. Biol. Chem. 271*, 11772–11780.

11. Zhao, J., Snyder, W. B., Muhlenhoff, U., Rhiel, E., Warren, P. V., Golbeck, J. H., and Bryant, D. A. (1993) Cloning and characterization of the psaE gene of the cyanobacterium *Synechococcus* sp. PCC 7002: characterization of a psaE mutant and over-production of the protein in *Escherichia coli. Mol. Microbiol. 9*, 183–194.

12. Antonkine, M. L., Jordan, P., Fromme, P., Krauss, N., Golbeck, J. H., and Stehlik, D. (2003) Assembly of protein subunits within the stromal ridge of photosystem I. Structural changes between unbound and sequentially PS I-bound polypeptides and correlated changes of the magnetic properties of the terminal iron sulfur clusters. *J. Mol. Biol. 327*, 671–697.

13. Jagannathan, B., and Golbeck, J. (2009) Breaking biological symmetry in membrane proteins: the asymmetrical orientation of PsaC on the pseudo-C_2 symmetric photosystem I core. *Cell. Mol. Life Sci. 66*, 1257–1270.

14. Jolley, C. C., Wells, S. A., Hespenheide, B. M., Thorpe, M. F., and Fromme, P. (2006) Docking of photosystem I subunit C using a constrained geometric simulation. *J. Am. Chem. Soc. 128*, 8803–8812.

15. Fromme, P., and Grotjohann, I. (2008) Structure of photosystems I and II. *Results Probl. Cell. Differ. 45*, 33–72.

16. Antonkine, M. L., Liu, G., Bentrop, D., Bryant, D. A., Bertini, I., Luchinat, C., Golbeck, J. H., and Stehlik, D. (2002) Solution structure of the unbound, oxidized photosystem I subunit PsaC, containing [4Fe-4S] clusters F_A and F_B: a conformational change occurs upon binding to photosystem I. *J. Biol. Inorg. Chem. 7*, 461–472.

17. Hubbell, W. L., Cafiso, D. S., and Altenbach, C. (2000) Identifying conformational changes with site-directed spin labeling. *Nat. Struct. Biol. 7*, 735–739.

18. Hubbell, W. L., Gross, A., Langen, R., and Lietzow, M. A. (1998) Recent advances in site-directed spin labeling of proteins. *Curr. Opin. Struct. Biol. 8*, 649–656.

19. Hubbell, W. L., and Altenbach, C. (1994) Investigation of structure and dynamics in membrane proteins using site-directed spin labeling. *Curr. Opin. Struct. Biol. 4*, 566–573.

20. Borbat, P. P., Costa-Filho, A. J., Earle, K. A., Moscicki, J. K., and Freed, J. H. (2001) Electron spin resonance in studies of membranes and proteins. *Science 291*, 266–269.

21. Meimberg, K., Fischer, N., Rochaix, J. D., and Muhlenhoff, U. (1999) Lys35 of PsaC is required for the efficient photoreduction of flavodoxin by photosystem I from *Chlamydomonas reinhardtii. Eur. J. Biochem. 263*, 137–144.

22. Vassiliev, I. R., Antonkine, M. L., and Golbeck, J. H. (2001) Iron-sulfur clusters in type I reaction centers. *Biochim. Biophys. Acta 1507*, 139–160.

23. Golbeck, J. H., Lien, S., and San Pietro, A. (1977) Isolation and characterization of a subchloroplast particle enriched in iron-sulfur protein and P_{700}. *Arch. Biochem. Biophys. 178*, 140–150.

24. Budil, D. E., Lee, S., Saxena, S., and Freed, J. H. (1996) Nonlinear-least-squares analysis of slow-motion EPR spectra in one and two dimensions using a modified Levenberg-Marquardt algorithm. *J. Magn. Reson. 120*, 155–189.

25. Kale, S., Ulas, G., Song, J., Brudvig, G. W., Furey, W., and Jordan, F. (2008) Efficient coupling of catalysis and dynamics in the E1 component of *Escherichia coli* pyruvate dehydrogenase multienzyme complex. *Proc. Natl. Acad. Sci. U.S.A. 105*, 1158–1163.

26. Hubbell, W. L., McHaourab, H. S., Altenbach, C., and Lietzow, M. A. (1996) Watching proteins move using site-directed spin labeling. *Structure 4*, 779–783.

27. McHaourab, H. S., Lietzow, M. A., Hideg, K., and Hubbell, W. L. (1996) Motion of spin-labeled side chains in T4 lysozyme. Correlation with protein structure and dynamics. *Biochemistry 35*, 7692–7704.

28. Mchaourab, H. S., and Perozo, E. (2000) Determination of protein folds and conformational dynamics using spin-labeling EPR spectroscopy, in Biological Magnetic Resonance (Berliner, L. J., Eaton, S. S., and Eaton, G. R., Eds.) pp 185–238, Kluwer Academic/Plenum Publishers, New York.

29. Jagannathan, B., and Golbeck, J. H. (2009) Understanding of the binding interface between PsaC and the PsaA/PsaB heterodimer in photosystem I. *Biochemistry 48*, 5405–5416.

30. Barth, P., Lagoutte, B., and Setif, P. (1998) Ferredoxin reduction by photosystem I from *Synechocystis* sp. PCC 6803: toward an understanding of the respective roles of subunits PsaD and PsaE in ferredoxin binding. *Biochemistry 37*, 16233–16241.

31. Rabenstein, M. D., and Shin, Y. K. (1995) Determination of the distance between two spin labels attached to a macromolecule. *Proc. Natl. Acad. Sci. U.S.A. 92*, 8239–8243.